UCRL-ID-146957

Metrology of Non-Rigid Objects

K. Blaedel, B. Swift, A. Claudet, E. Kasper, S. Petterson

January 1, 2002

U.S. Department of Energy

Lawrence
Livermore
National
Laboratory

DISCLAIMER

This work was performed under the auspices of the U. S. Department of Energy by the University of California, Lawrence Livermore National Laboratory under Contract No. W-7405-Eng-48.

Metrology of Non-Rigid Objects

Ken Blaedel, David Swift, Andre Claudet
Lawrence Livermore National Laboratory
Livermore, CA

Eric Kasper
Cal Poly State University
San Luis Obispo, CA

Steve Patterson
University of North Carolina, Charlotte
Charlotte, NC

January 2002

Problem Definition

Dimensional characterization of non-rigid parts presents many challenges. For example, when a non-rigid part is mounted in an inspection apparatus the effects of fixturing constraints are significant. If the part is not used in normal service with the same load conditions as during inspection, the dimensional characteristics will deviate from reported values. Further, the solution of designing specialized fixturing to duplicate "as-installed" conditions does not fully resolve the problem because each inspection requires its own methodology. The goal of this project is to formulate the research problem and propose a method of assessing the dimensional characteristics of non-rigid parts.

The measured dimension of a rigid component is traceable at some level of confidence to a single source (NIST in the USA). Hence the measurement of one component of an assembly can be related to the measurement of another component of that assembly. There is no generalized analog to this pedigreed process for dimensionally characterizing non-rigid bodies. For example, a measurement made on a sheet-metal automobile fender is heavily influenced by how it is held during the measurement making it difficult to determine how well that fender will assemble to the rest of the (non-rigid) car body. This problem is often overcome for specific manufacturing problems by constructing rigid fixtures that over-constrain the non-rigid parts to be assembled and then performing the dimensional measurement of the contour of each component to check whether each meets specification. Note that such inspection measurements will yield only an approximation to the assembled shape, which is a function of both the geometry and the compliance of the component parts of the assembly. As a result, non-rigid components are more difficult to specify and inspect and therefore are more difficult to purchase from outside vendors compared to rigid components. The problems are compounded as the requirements come to include higher and higher precision.

The central idea for this project is the concept of a "free shape." The free shape is the geometry of the part when no loads are present. That is, when those loads produced

by fixturing, gravity and others are not present. Since it is impossible to directly measure the free shape, some method for inferring it must be developed. Once the free shape is known some metric must be developed for acceptance or rejection of the part.

Applications

Within LLNL

The non-rigid metrology problem is of direct interest to the laboratory in at least three ways. First, it has implications concerning the characterization of thin, hemispherical shells. Second, it has application to the metrology of thin photomasks for extreme-ultraviolet lithography (EUVL). Third, it can help in the inspection of potassium dihydrogen phosphate (KDP) crystals in advanced laser systems. It is important to industry because it has applications to metrology of sheet-metal parts.

Metrology of Hemi-Shells

The Stockpile Stewardship Program demands a better understanding of the deformation that occurs in hemi-shells resulting from their manufacture and assembly. Hemi-shells are non-rigid bodies, which for example, deform under their own weight and are easily deformed by fixtures that hold them during the manufacturing process. In order to inspect a hemi-shell, it is constrained in a fixture that "rounds up" the equator of the shell and thus purposely removes some of the deformation of the shell that results, for example, from non-uniform residual stress.

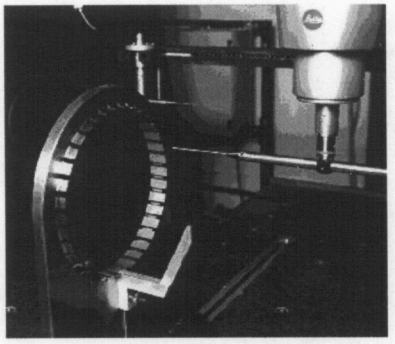

Figure 1: Over-constraining Fixture

Figure 1 illustrates a fixture that over-constrains a hemi-shell. The inspector can then compare the measurement of the constrained shell and the drawing of a perfect shell and determine, within some uncertainty, whether it is acceptable or not. A number of problems arise from using such fixtures. One is that the fixture, which over-constrains the shell, imposes ill-defined constraints on the shell. Hence, slight variation in the procedure or conditions of the measurement introduces uncertainty into the dimensional measurement. In addition, the fixturing and measurement processes that have arisen at the different agencies within the DOE complex are unique to each agency and the measurement data are not traceable from one institution to another.

EUVL Photomasks

EUVL photomasks are high aspect ratio optics subject to deformation by external forces. The error budgets for image placement error for EUV Lithography dictate that a mounted mask be flat. One contributor to non-flatness in the clamped state is the freestanding non-flatness of the mask itself, which is further influenced by the non-flatness of the mask substrate. The SEMI P37 specification for EUVL masks contains a global P-V flatness value for the unclamped state. While the P-V value does guarantee that the mask will perform, producing masks to meet this is very difficult.

A relaxed specification based on the free-shape that still guarantees performance while easing the manufacturing requirements is desirable. For example, if inferences can be made on the clamped geometry based on the unclamped geometry then suppliers would be able to more easily produce mask substrates. This translates directly into lower costs for the mask production.

KDP Crystals

Thin, high precision KDP crystals are used in NIF. Crystals are manufactured in the constrained condition. The final thickness of the finished crystal is approximately 1.0cm. With a width and height of 42 cm, KDP crystals have an aspect ratio that makes them very non-rigid.

The finished crystals are inspected in a vertical, freestanding condition using optical techniques. The crystals are then edge constrained for use at a variety of angles relative to gravity. The combined effects of gravity loading and constraint induced errors turn out to be one of the dominant sources of error affecting the performance of the crystal. Extensive modeling and analysis has been performed to better understand these effects while attempting to improve on them in the mechanical design.

A method for assessing the constraint system and the influence of gravity and other boundary conditions would greatly improve the ability to predict and/or improve performance of NIF KDP crystals.

Outside LLNL

Many examples of non-rigid bodies exist in industry. Most any sheet metal part is easily deformed under small loads. Space based optics have conflicting goals of stiff and lightweight design.

Sheet Metal

Sheet metal parts are common. For example, automotive body panels must have precise geometry for aesthetic reasons. Elaborate, specialized fixturing devices and metrics are used for characterization. A generalized method for assessing the dimensional characteristics of the parts would provide for a more flexible metrology process.

Space Based Optics

One design parameter for space-based optics is total mass. The optics must be lightweight to facilitate transportation into orbit. Thus, the option of adding material to increase rigidity is not available. Although the operating environment for the optics does

not require the same rigidity as for earth-based optics, they are manufactured and inspected in the same manner. The ability to measure while the optic is under the influence of gravity and predict its shape with gravity removed would provide better insight into its the future performance.

Technical Approach

The method begins with a measurement of the non-rigid part as it is exactly constrained under well-defined conditions and, in contrast to current convention, is not measured in an over-constrained condition. The deformation imposed by the well-defined constraints can then be removed by simulation to predict the shape of the part as though it were free from external forces. This condition, which is not physically realizable, is then used to decide on the acceptability of the component part and further, to estimate the shape of an assembly of non-rigid component parts. The acceptability of the part now concerns not just how close the geometry of the freestanding part is to the geometry of the ideal part in the specification, but also includes the nature of the forces required to make the constraint-free part conform to the specification geometry. A further advantage of this approach is that two such components can be assembled to each other by simulation because both the geometry and the compliance of the components are known and available to the simulation.

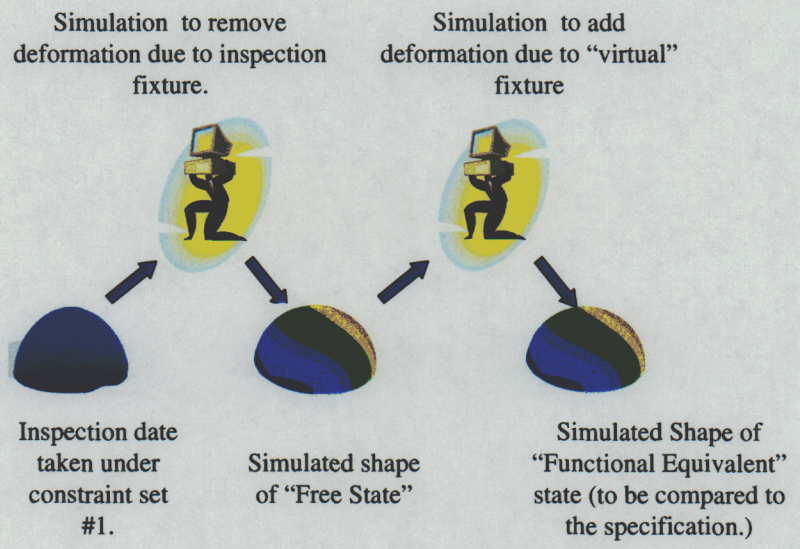

Figure 2: Technical Approach

In essence, the part is measured and then compared to specification through the use of a "numeric fixture" rather than being measured and then compared to a specification through the use of a "hard fixture". The approach is illustrated in Figure 2.

Method of Modeling or Simulating the Deformation Due to Fixturing

Finite Element Analysis

Finite element method is the simplest way to model and simulate the deformations of thin shells subject to various boundary conditions. The models can be built using various elements described in the previous sections. Commercial and homemade finite element codes are used to simulate the results for thin shell problems in this project. The commercial codes considered for use on this project are Pro Mechanica, ANSYS, ABAQUS, and COSMOS. The homemade finite element codes considered for this project are Nike, and FEAP (a simple Fortran FEA code). Nike is a finite element code that has been developed for internal use at Lawrence Livermore National Laboratory. These codes are used to check and verify the consistency of the results of each code relative to another. Pro Mechanica, ABAQUS, COSMOS, and FEAP were selected for use on this project.

Close Form Solution

Closed form solutions were also evaluated for this project. The selection of load cases for the actual experiment does not have closed form solutions but simpler load cases were evaluated and compared to the results of the FEA. An example of a simple load case that has a closed form solution is a cylinder with a uniform pressure applied to the inner or outer surface. Comparison of results between this simple load case and the FEA results allowed the experimenters to eliminate Pro Mechanica as a viable option for this project. Pro Mechanica produced results that were inconsistent with closed form results and the other FEA codes.

Uncertainty in the Process

In order to increase the usefulness of reported measurement values a statement of uncertainty must be included. Thus, the many contributors to the overall uncertainty must be assessed. In addition to the typical uncertainties associated with data acquisition (hardware), there is additional uncertainty associated with the FEA. A "home grown" FEA code was used for this work. Thus, more complete knowledge of the underlying operations and the associated uncertainty was realized. Significant contributors to the overall uncertainty are given below.

Material Properties

Assigning material properties to an element in an FEA study makes the significant assumption that the part model being analyzed has the same material property as the actual part. It is typically assumed that the parts will be homogeneous and isotropic. In most instances these assumptions are not completely accurate. These assumptions result in uncertainty in the FEA results. The effect of variation in the material properties on the FEA results can be determined. For example, the Young's modulus is directly proportional to deflection. Thus, if the Young's Modulus varies by 20%, then deflections can also vary by 20%.

Standard tensile tests can accurately measure the Young's modulus of a material to about 1%. The accuracy is worse for determining Poisson's ratio as a result of the uncertainties in measuring lateral displacement. Ultrasonic methods for measuring mechanical properties have been explored and results show improved accuracy in the determination of mechanical properties. The fundamental principle is measurement of ultrasonic velocities generated by a dynamic pressure wave into a material of known thickness and measuring the transit time of the emerging acoustic pressure wave. The uncertainty in Young's modulus calculation based on this based is dependent on the density of the material and the thickness of the medium. The Young's modulus' calculated uncertainty based on uncertainties in thickness and density is determined to be around 0.4%. This uncertainty is improved to 0.2% with improved density measurement. Detailed results for this calculation are given in Appendix A.

Mesh

The accuracy of the solution is dependent on the quality of the mesh. The FEA convergence is also greatly affected by the mesh quality. The global displacement should converge to a stable value and any results of interest should converge locally. A more subjective measure of the quality of the mesh is its appearance and ability to visually convey the geometry it represents. Typically, the better-looking mesh is better and a bad-looking mesh almost always indicates a problem. Equilateral triangles and squares are the ideal elements to use with smooth and gradual transitions without skinny, distorted elements. The type of elements used (i.e. p-elements or h-elements) is also a factor in mesh density. The use of higher order p-elements does not require as dense a mesh as same h-elements for the same model. P-elements allow for higher edge polynomial orders which can improves the representation of the load curvature.

Boundary Conditions

Boundary conditions are difficult to model since physical interactions of constraints and modeled geometry are complex. For the purposes of experimental validation it is possible to design geometry and fixtures to create boundary conditions that are more accurately modeled. This has been achieved by producing boundary conditions that have very little friction. An exact constraint fixture also greatly reduces the unknown forces acting on the model.

Linear Static Assumption

Linear static solutions are most common solutions available when using finite element analysis. The popularity of this solution often obscures the fact that it represents a significant assumption of linear events. Linear event are typical idealized in most problems and do not typically exist. However, linearity in thin shell analysis is a good assumption because of low-stress condition that is created during bending of the shell. Thin shells are used to experimentally validate the process for this work.

Element Type

When using finite element analysis different element types can be used to model thin shells. Two candidate elements for this work are shell elements and hexahedral solid

elements. Shell elements typically represent thin-walled structures. They can be quadrilateral or trilateral. A quadrilateral mesh is usually more accurate mesh of similar density based on trilateral elements. Most preprocessors can mesh a surface with quads only or apply a quad dominant mesh where triangles are used only when the mesher cannot resolve an area within specified element tolerances. Triangles are acceptable in regions of gradual transitions. Linear or first order shell elements are normally planar and degrade in accuracy as their initial definition deviates from planar. This is an issue only for quad elements because a three-noded triangle must be planar. Higher order shell elements can provide accurate results with curved initial geometries. A benefit for using higher order elements is that positioning the mid-side nodes on the actual curved geometry increases the model's accuracy. P-elements are ideal to represent bi-directional curvature and can smoothly represent initial geometry.

Most first order triangle element are only capable of calculating a single strain value across the entire element. Consequently, they are known as constant strain elements. This limitation can lead to overly stiff results under a given load as localized strain gradient will be difficult, if not impossible, to capture. They do provide adequate results when used on flat or gently curving surfaces with minimal strain variance across the span. Linear quad elements have a linear strain distribution from one node to the next so they are better at capturing localized stresses. Adding mid-side nodes to both these elements improves their strain distribution by a polynomial order.

Ill-Condition Stiffness Matrix

Ill-condition stiffness matrix results in solutions that could be an order of magnitude different in value from a few percent change in the stiffness coefficient matrix. In matrix terminology, the rows of an ill-conditioned matrix are almost linearly dependent. For a 2 by 2 systems, this means that the second row of the coefficient matrix is almost a scalar multiple of the first row. In structural terminology, a major cause of ill-conditioning in practical finite element models is a large different in stiffness with the stiffer region being supported by the more flexible region. This circumstance shifts essential numerical information to the latter digits of stiffness coefficient Kij. These latter digits may be so few in number that the solution in worthless. Physically, the stiffer region has one or more displacement states that are almost rigid-body motions within a more flexible supporting structure. The limiting case in a structure without any supports: it has only rigid-body motion in static analysis, and its stiffness matrix is singular.

In this particular study this problem can be encountered when a flexible shell element is modeled and it is connected to a stiff boundary condition. This can result in high unrealistic deflections at the node. This problem can be mitigated by distributing the loading at number of nodes around the boundary condition as oppose to a single node connection.

A numerical measure of ill-conditioning in a coefficient matrix is the condition number. A large condition number denotes an unstable solution and warns that a finite element solution may contain appreciable error. The condition number of matrix K (stiffness matrix) is simply defined as (1),

$$C(\mathrm{K}) = \frac{\lambda_{\max}}{\lambda_{\min}} \qquad (1)$$

where λ_{max} and λ_{min} are the largest and smallest eigenvalues of matrix K. It can be shown that for each power of ten in the ratio $\lambda_{max}/\lambda_{min}$, the operations of equation solving lose about one digit of accuracy in the displacement mode associated with λ_{min} (Cook, 1989). The estimated accuracy loss is (2).

$$\text{accurate digit loss} \approx \log_{10} \frac{\lambda_{max}}{\lambda_{min}} = \log_{10} C . \qquad (2)$$

For example, for C(K)=105, if computer has seven-digit capacity, only two digits are reliable in the computed displacements. With sixteen-digit capacity, eleven accurate digits remain.

Uncertainty Management

An effective measurement requires management of uncertainty. Once the uncertainty contributors are identified steps can be taken to minimize their magnitude. For this work action is required on both the data acquisition (hardware) and analysis (software) sides. On the hardware side, multiple measurements are taken and the fixturing forces and displacements are recorded. To facilitate the analysis, the cylinder is measured close to its free shape the material properties are measured.

Table 1: Uncertainty Contributors

Source of Uncertainty	Magnitude of Uncertainty	Remedy
Cylinder wall de-center	2μm	Measure surfaces independently
Axial coordinate measurement	0.5mm	Use different measuring machine
Idealized vs. Exact Geometry	8 parts in 100	Use "Exact" geometry
Element Domain – n Flat Facets	1-cos(pi/4n)=1e-7	Use Curved Elements for n>36
Mesh Properties	Log(C/[K])	Avoid Ill-Conditioned K-Matrix
Localized Contact at Boundary	14 parts in 100	Exclude Local Contact Area
Isotropic Material Properties	4 parts in 1000	Improve Material Testing
Material Orthotropy	Moderate	Improve Material Testing
Element Type Selected	Moderate	Select Problem Specific Elements
Numerical Integration	Zero	Linear Map Elements to Model Space

Table 1 illustrates some uncertainty contributors and suggestions for remedying them.

Experimental Demonstration

A copper thin walled cylinder was manufactured under carefully controlled conditions. A cylinder was chosen because of its manufacturability and because it can be oriented so that gravity has little effect. The goal of the design was to reduce the uncertainty in the measurement to small values compared to those for FEA.

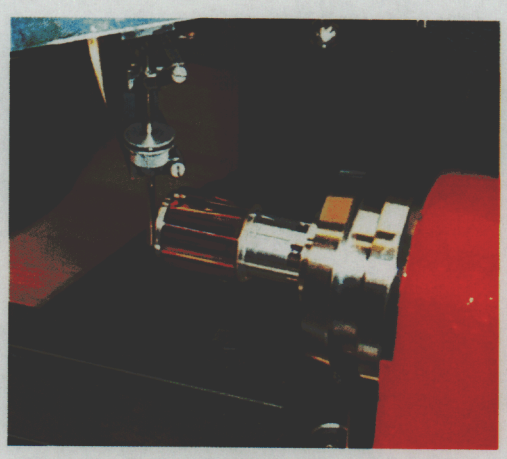

Figure 3: Test Cylinder Manufacturing

Figure 3 shows the cylinder at an intermediate step in the manufacturing process. A fixturing device was built to exactly constrain the cylinder. The design facilitated readings of both displacements of the cylinder and reaction forces at the constraints.

Figure 4: Test Artifact Fixture

The actuators on the fixturing device deformed the cylinder approximately 2% of its wall thickness over 15 steps. Measurements of the displacement were obtained by placing the entire fixturing device on a Tropel CylinderMaster 25 cylinder inspection device.

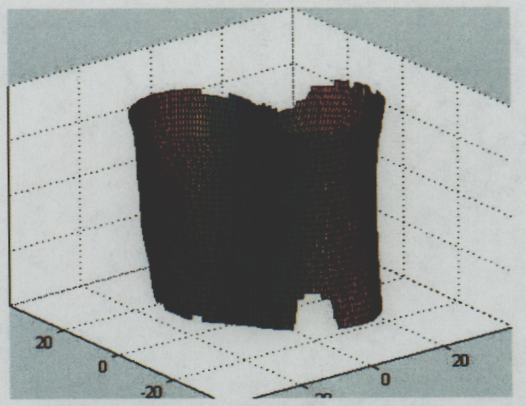

Figure 5: Exaggerated Deformations

Figure 5 illustrates the deformations (exaggerated) induced by the fixture. The fixture contacted the cylinder at 3 points and produces a tri-lobe deformation.

Measurement Data Analysis

The goal of the numerical simulation section is to determine the stress-free configuration for the test cylinder from a given set of experimental data. The experimental data was determined based on a set of sequential optical measurements. The experimental data was determined follows: first, the test cylinder was set on a loading fixture and an initial radial deviation map is obtained, denoted as ΔX_0. The test cylinder was then incrementally displaced at three points on the outer surface of the cylinder and the corresponding radial deviations are recorded. A maximum radial displacement of approximately 2% of the wall thickness is imposed over 15 increments.

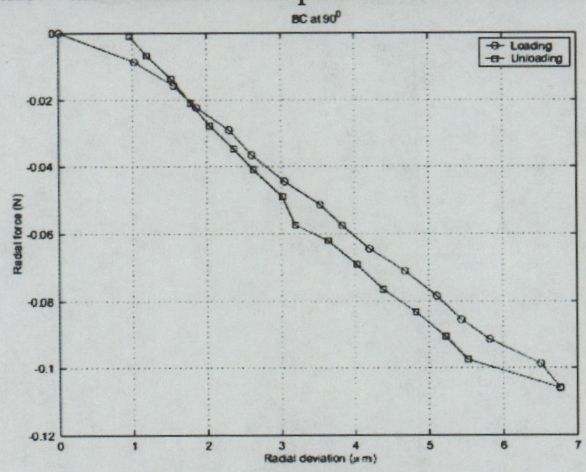

Figure 6: Load-Displacement Curve at 90° Displacement Boundary Condition

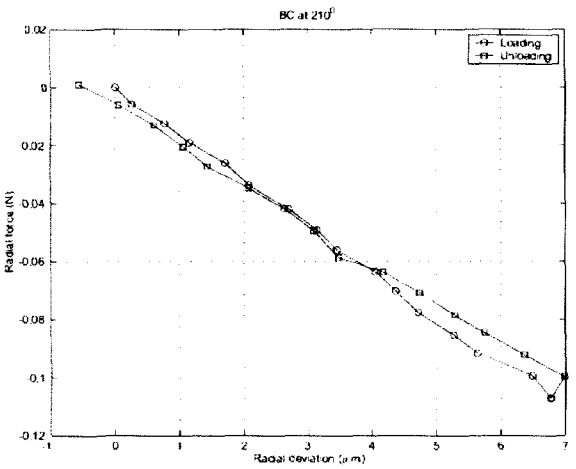

Figure 7: Load-Displacement Curve at 210° Displacement Boundary Condition

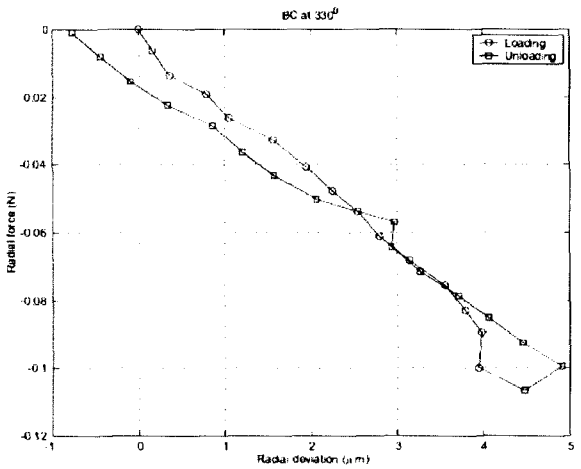

Figure 8: Load-Displacement Curve at 330° Displacement Boundary Condition

A plot of the radial force versus radial displacement for each of the three boundary conditions is shown in Figure 6 through Figure 8. As shown from Figure 6 through Figure 8 the response is linear and returns to its initial state to within the uncertainty of the optical measurements. Given the linearity and the inherent elasticity of the load-deflection curves a linear-elastic shell formulation was used for the numerical simulations. In addition, it is also assumed that the elastic material properties and wall thickness are known and constant throughout the deformation.

An overview of the procedure used to determine the stress-free state is given below.

- The initial finite element discretization was determined by superimposing the experimental radial deviation map in the unloaded configuration, ΔX_0, to the geometry of a "pure" right circular cylinder, X_0. The resulting initial finite element discretization is denoted as $X = X_0 + \Delta X_0$.

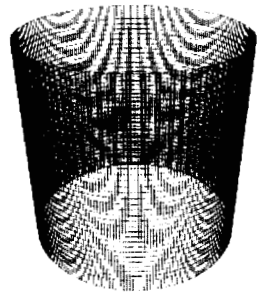

Figure 9: Finite Element Mesh Discretization, 256x35

Note the grid resolution of the experimental data and the finite element discretization coincide, specifically the grid consists of 256 data points around the circumference and 35 data points along the longitudinal axis of the cylinder, see Figure 9.

- Since the discretization of the experimental data and the finite element mesh coincide the prescribed normal displacement boundary conditions correlate directly to the experimental data.

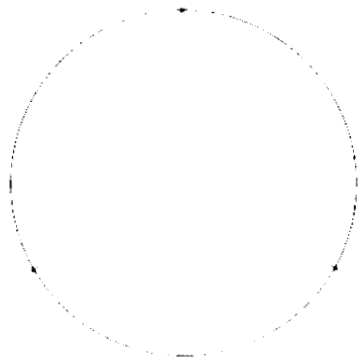

Figure 10: Locations of the Radial Boundary Conditions

The loading fixture imposes a prescribed normal displacement (over 15 increments), of approximately 2% of the wall thickness, to the outer surface of the cylinder at three locations equally spaced. Figure 10 illustrates the radial displacement boundary conditions.

- Given the initial finite element discretization, X, and the three displacement boundary conditions (based on the experimental data) contour maps of the radial displacement for the experimental and a preliminary finite element simulation can be plotted.

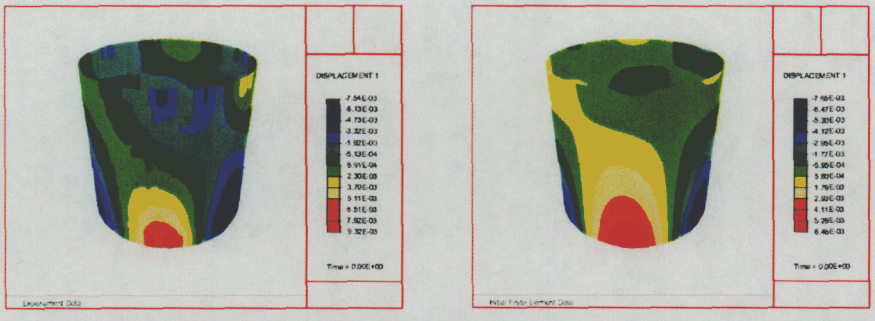

Figure 11: Contour Plot of Radial Displacements for the Experimental Data and Initial Finite Element Discretization. Units are mm.

Figure 11 shows the contour maps. Note that both the experimental and numerical results are based on the same initial configuration.

- Recall the goal is to minimize the error between the deformed coordinates of the finite element discretization to that of the experimental data. To obtain this minimization a simple coordinate update scheme shown below is utilized.

  1. Initialize iteration counter k=0
  2. Set current coordinates $x^{(k+1)} = X$
  3. Solve for the nodal displacements $u^{(k+1)}$,

     $$u^{(k+1)} = K^{-1}\left(x^{(k+1)}\right)R,$$

     where K is the tangent matrix and R is the residual vector.
  4. Update iteration counter k=k+1
  5. Update the coordinates by setting $x^{(k+1)} = x^{(k)} + \left(\Delta X - u^{(k)}\right)$ where ΔX is the difference in the initial and final configurations (loading portion of the curve) of the experimental data.
  6. Solve for the displacements, $u^{(k+1)}$, as

     $$u^{(k+1)} = K^{-1}\left(x^{(k+1)}\right)R$$

  7. Check for convergence

     $$r = \left\| u^{(k+1)} - u^{(k)} \right\|$$

  8. If (r>TOL) repeat from (4) or else finish and report $x=u^{(k+1)}$

- Once convergence is achieved then the updated coordinates, x, are stored. Note using an initial finite element discretization with coordinates, x, and imposing the

experimental displacement boundary conditions the final deformed configuration of the numerical model will approximate the deformed configuration of the experimental data to within the uncertainty of the data. The stress-free configuration is then obtained by unloading the radial displacement boundary conditions or simply x.

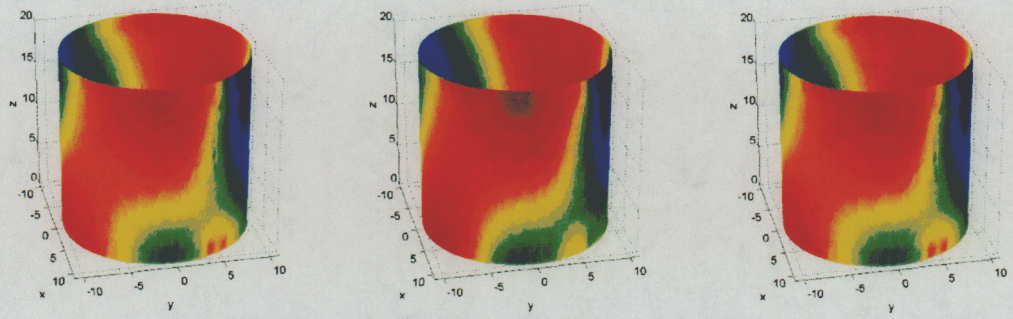

Figure 12: Contour Plots of the Radial Coordinates for the Experimental Data, Initial Finite Element Discretization and Final (Stress Free) Discretization

A three-dimensional contour map of the deformed radial coordinates for the experimental, initial (i.e. initial iteration) finite element analysis, and the final (i.e. converged) finite element analysis are shown in Figure 12.

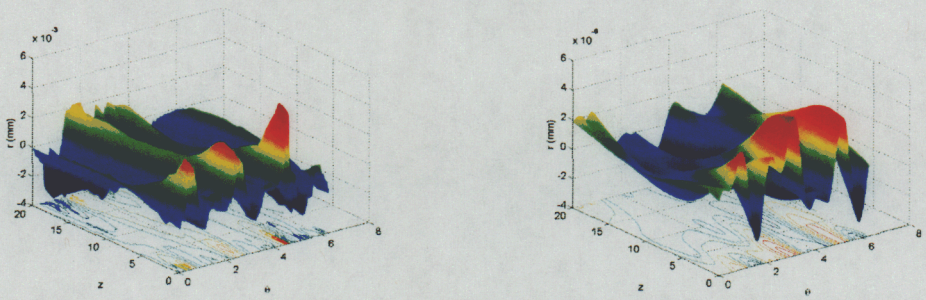

Figure 13: Contour Plots for the Error in Radial Coordinates of the initial and Final (Stress Free) Discretization Referenced from the Experimental Data

In addition, Figure 13 shows the error in the deformed radial coordinate for the cases above.

- Figure 14 depicts the initial configurations for the experimental data and the computed stress-free finite element data.

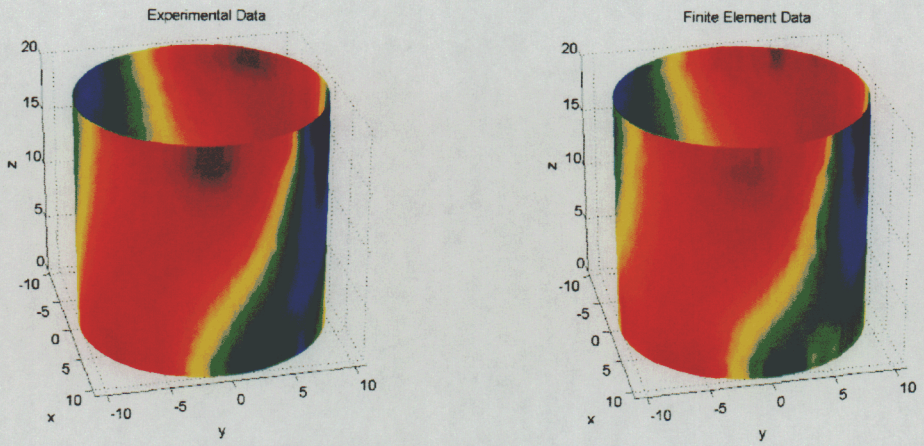

Figure 14: Contour Plots of the Radial Coordinates for the Initial Experimental and Stress Free Finite Element Data

To assess the uncertainty of the optically measured cylinder data to that of a "perfect" or "pure" cylinder and the stress-free configuration developed from the finite element analysis several scalar measures were utilized.

Table 2: Scalar Measures

Description	N_1 (mm)	N_2 (mm)	ε_1 (N-mm)
Comparison of the experimental and finite element data	5.467×10^{-6}	1.158×10^{-4}	--
Comparison of the experimental and pure cylinder data	1.883×10^{-2}	5.156×10^{-1}	--
Stress-free finite element configuration to initial experimental configuration	--	--	7.632×10^{0}
Stress-free finite element configuration to initial pure cylinder configuration	--	--	1.047×10^{1}
Initial experimental configuration to pure cylinder configuration	--	--	2.217×10^{0}

Table 2 lists the various scalars used, specifically an infinity norm defined as (3),

$$N_1 = \max\left|R_{ij}^{\exp} - R_{ij}^{fea}\right| \text{ or } N_1 = \max\left|R_{ij}^{\exp} - R_{ij}^{pure}\right| \qquad (3)$$

where R_{ij} is the deformed radial coordinates associated with the discretization, the superscript *exp* denotes the experimental data, *fea* denotes the final finite element data, and pure denotes the data for a pure or perfect cylinder. The 2-norm defined as (4),

$$N_2 = \left[\sum_i \sum_j \left(R_{ij}^{\exp} - R_{ij}^{fea}\right)^2\right]^{\frac{1}{2}} \text{ or } N_2 = \left[\sum_i \sum_j \left(R_{ij}^{\exp} - R_{ij}^{pure}\right)^2\right]^{\frac{1}{2}} \qquad (4)$$

and the last scalar measure is an energy term, ε_1, which is defined as the work required (*i.e.*, radial force * radial distance) to deform a given initial configuration (*e.g.*, the pure cylinder configuration) to another initial configuration (*e.g.*, the stress-free finite element configuration).

Acceptance of Non-Rigid Parts

In the case of conventional rigid-body inspection, the measurement of a part is directly compared with drawing of ideal part and, if the measurement with its uncertainty falls within the specified drawing tolerances, the part is declared acceptable. The implicit assumption is that the part is not deformed in inspection, assembly or use. For non-rigid parts, the same basic acceptance approach applies, but a predicted shape rather than the measured shape is used as a comparison with/to the ideal shape given on a drawing. Referring to Figure 2, upon "removing" the constraints imposed during measurement, a new set of constraints is imposed upon the simulated free-state shape that reflect how the part is to constrained in its functional state. The resultant shape with its associated uncertainty is then compared to the specification, which is still often embodied as a drawing. A decision must now be made whether the part is acceptable or must be rejected. Thus the acceptance of a non-rigid part contains the extra steps of removing the measurement constraints and applying functional constraints. In practice, the two steps could be combined, but keeping them separate makes for clearer discussion.

Consider first the degenerate example of a space-based optical surface that is mounted to exactly constrain its six rigid-body degrees of motion. It is specified to take a well-defined shape, within an allowable tolerance, which is given by a drawing. While this case is conceptually identical to the rigid-body case, it is in practice quite different. The difference between the rigid body and the non-rigid part lies in the additional uncertainties that arise in using FEA to predict its free-state shape, that is, the shape it will take in space. Here, the free-state shape and the shape it takes in service (i.e., the functional shape) are the same.

Consider as a second case, the hemispherical shell described above, whose outer contour is required to be spherical to some tolerance when it is assembled to a hemispherical mate. In current practice, in order to inspect a hemishell, the equator is forced to be round, then the diameter is measured and the outer contour is measured in this constrained state. In essence, the rounding ring is used to bring the part into its functional state, that is, the assembly process is "simulated" by forcing a "rounding ring" over the equator of the part. In this case, requiring the free-state shape of the shell to be spherical would cause the rejection of many useable and functional parts. As described above, the problem with using a rounding ring is that it introduces unknown constraint conditions on the part that are quite different from what it may see in assembly. For example, the process of forcing the rounding ring over the equator tends to trap friction between rounding ring and hemishell, which results in deformation of the outer contour. Thus a perfect part may be rejected because of the friction associated with using the rounding ring. Also, any mismatch in the circumference of the rounding ring and the length of the equator of the part causes significant radial forces and moments about the equator and concomitant deformation of the outer contour.

An alternative approach to using a hard fixture to round up the equator is to use a "soft" fixture, which does not suffer a number of the shortcomings of the hard fixture. The soft fixture is a finite element simulation of the ideal hard fixture. The soft fixture simply represents a hard fixture that is free of friction between the fixture and part free of any mismatch between the length of the equator of the part and the circumference of the fixture.

Consider as a third case, the photomasks described above, which are required to be flat to some tolerance as they are sequentially mounted in an exposure tool. In this case, requiring the free-state shape of the photomask to be flat is again overly restrictive because the mounting process has some capability to flatten the mask. Because a photomask is almost planar, it can be measured with its patterned surface in a vertical plane and thus the deformation due to gravity becomes extremely small. Hence, the inspected state is very close to the free-state shape. (This is unlike the hemishells, which sag under gravity regardless of how they are oriented or fixtured.) However, the photomasks for EUVL are used in vacuum with their front surface in a horizontal plane. The gravity-induced sag of a photomask on three-point support is approximately ten times the allowable departure from flat. Thus the mask is mounted against a flat-faced, electrostatic chuck. The chuck therefore has a limited capability to "flatten" the mask.

One method of inspecting photomasks is to mount them to an "inspection chuck", one that replicates the actual chuck in the exposure tool, and then measure the resultant flatness. As with the hemishell inspection, the hard fixture suffers from practical shortcomings. One example is that if a particle becomes trapped between the chuck and the photomask, then the deformation that is caused by the particle would cause the rejection of a good photomask.

An alternative approach to using a surrogate chuck, i.e., a hard fixture, to flatten the photomask for inspection is again to use a "soft" fixture. The soft fixture is a model of the flattening ability of the chuck. In this case, a FEA is performed of constant pressure acting to deform the photomask against a rigid, flat plane. Applying this model to a freestanding photomask allows the inspector to determine whether the mask will be flattened within the flatness specification and hence accept a mask, or whether it is deformed such that it cannot be flattened, in which case it should be rejected.

As a fourth example, reconsider the case of the assembly of two hemishells into a spherical shell, that is, the assembly of two non-rigid parts. Here, it is difficult to determine, a-priori, if the resultant assembly will meet a geometric specification. The best way is to perform the assembly and then inspect it. If the inspection fails, it is difficult to diagnose the cause.

Conclusion

The problem of metrology of non-rigid objects is complex. There is no pedigreed process as with rigid artifacts. The problem is encountered in normal industrial operations such as sheet metal processes but often addressed in non-generalizable methods. Further, it is encountered in precision engineering because, at some level of precision, everything is non-rigid.

This work provides new insight into the metrology of non-rigid objects. The research problem has been identified – a significant contribution in itself. A method to address the problem was formulated and demonstrated experimentally on a thin walled

copper cylinder. The free shape was determined and several acceptance metrics computed.

Assessing the uncertainty in the non-rigid metrology process is a complicated issue. In addition to the typical uncertainty associated with the data acquisition there is uncertainty introduced with the computational analysis. Factors contributing to the overall uncertainty were identified and the relative contributions for many of them were quantified.

The results of this work have applications in several areas. At LLNL, the results can be used by EUVL for photomasks. NIF can also benefit by using the techniques to characterize KDP crystals. The original motivating problem, metrology of hemi-shells is possible, but not currently a priority with the customer. The clear posing of the research problem makes the issue more salient. This may lead to the desirable outcome of increased industrial research in the area.